Article

Can the MODIS Data Achieve the Downscaling of GOME-2 SIF? Validation of Data from China

Haixiang Si [1] , **Ruiyan Wang** [2,*] , **Ruhao Wang** [1] **and Zixuan He** [1]

[1] College of Resources and Environment, Shandong Agricultural University, Tai'an 271018, China; haixiang_si@163.com (H.S.)
[2] National Engineering Research Center for Efficient Utilization of Soil and Fertilizer Resources, Shandong Agricultural University, Tai'an 271018, China
* Correspondence: wry@sdau.edu.cn

Abstract: Solar-induced chlorophyll fluorescence (SIF) can accurately reflect the photosynthetic capacity of vegetation and information on the physiological status of vegetation, which is of great research significance and application value. However, the low resolution of the solar-induced chlorophyll fluorescence product of the inverse performance makes it difficult to perform fine-scale studies. Therefore, concerning the above problem, this study proposes a random-forest-based downscaling method based on random forest. We used MODIS reflectance data to analyze GOME-2 SIF data at 0.5° resolution over the Chinese mainland in 2011 and created a monthly SIF product at 0.05° resolution for the Chinese mainland through downscaling. Then we performed a veracity check on the downscaled SIF data, analyzed factors (land cover type, climate zone type, and DEM) that could affect its accuracy, and explored the feasibility of using MODIS data in future GOME-2 SIF downscaling studies. The results show that the downscaled SIF is in remarkable agreement with the GOME-2 SIF, with an improved spatial resolution from 0.5° to 0.05°, and that the structural and physiological information of the SIF is well represented in the downscaled SIF, which is essential for assessing global photosynthesis. In addition, in the region with grassland land cover type, temperate grassland climate region, alpine vegetation climate region of Qinghai–Tibet Plateau, as well as the region with high altitude and complex terrain, the accuracy of using MODIS to downscale the GOME-2 SIF data is low.

Keywords: GOME-2 SIF; downscaling; solar-induced chlorophyll fluorescence; authenticity check

1. Introduction

Solar-induced chlorophyll fluorescence (SIF) can accurately reflect information on the photosynthetic capacity and physiological status of vegetation, and can be used as an indicator of plant health, which has important research significance and application value [1–3]. Remote sensing of solar-induced chlorophyll fluorescence is an emerging vegetation remote sensing technique that has been developed in recent years. The use of SIF remote sensing can make up for the shortcomings of traditional vegetation remote sensing observations of vegetation and provide new ideas and techniques for the monitoring of global terrestrial ecosystems [2,4,5]. In recent years, scholars from various countries have carried out many related studies on chlorophyll fluorescence remote sensing. Based on the high-resolution spectrum of the Fourier Transform Spectrometer (FTS) mounted on GOSAT, Joiner [6] used the Fraunhofer line near 770 nm to obtain chlorophyll fluorescence information and related parameters by using the least square fitting method, and plotted the global chlorophyll fluorescence distribution. Guanter [4] used the simulated data of the FLEX satellite and based on the improved SFM algorithm obtained the SIF inversion results of the O_2-A and O_2-B bands. Using GOSAT satellite data, Liu and Liu [7] created a least-squares fit-based chlorophyll fluorescence inversion algorithm using the Fraunhofer line in the range around 770 nm with the help of high-resolution solar irradiance spectra, and thus

obtained chlorophyll fluorescence information for the Chinese region. Wen [8] generated a high spatial resolution SIF dataset from 2002 to the present based on the SCIAMACHY SIF and GOME-2 SIF original datasets provided by Joiner and the GFZ scientific research team. At present, there are many retrieval products of solar-induced chlorophyll fluorescence, such as GOME-2 SIF, OCO-2 SIF, and TROPOMI SIF [9–11]. However, most of these datasets suffer from low spatial resolution and poor spatial continuity, which pose significant challenges for global applications.

To overcome the challenges posed by low spatial resolution and poor spatial continuity of existing SIF data products, researchers have employed physical models and machine learning methods to downscale the data. In essence, SIF downscaling involves using a predictive model that leverages coarse-resolution SIF data as training samples and one or more high-resolution ancillary data sources (such as reflectance) to generate fine-scale SIF products. Yu [12] generated a spatially continuous 0.05° global daily average OCO-2 SIF data product based on the OCO-2 SIF dataset provided by NASA. Duveiller [13] improved the spatial resolution of GOME-2 SIF data from 0.5° to 0.05° by using a nonlinear downscaling function. Li and Xiao [14] proposed a new OCO-2 SIF dataset with a spatial resolution of 0.05° using the Cubist regression tree model. Hu and Mo [15] conducted a downscaling study on GOME-2 SIF data based on the statistical relationship between SIF and normalized difference vegetation index (NDVI), increasing its spatial resolution from 0.5° to 0.05°. Downscaling of SIF data has been extensively studied, with most approaches utilizing MODIS data and other ancillary variables as input. However, there is a paucity of research on the feasibility of using MODIS data for downscaling SIF data and on the validation of downscaled SIF data.

Therefore, this study proposes a downscaling method based on a random forest algorithm to generate monthly scale continuous downscaled SIF data of 0.05° for the Chinese mainland (excluding Hainan, Taiwan, Hong Kong, and Macao Special Administrative Regions) using the 2011 GOME-2 SIF dataset and MODIS reflectance data. Then we perform a veracity check on the downscaled data, analyze factors that may affect downscaling accuracy (land cover type, climate zone type, and DEM), and explore the feasibility of MODIS data in GOME-2 SIF downscaling studies.

2. Study Area and Data

2.1. Overview of the Study Area

China is located in the northern hemisphere, east of the Eurasian continent, on the west coast of the Pacific Ocean, bordering the sea in the southeast, and extending inland in the northwest. The terrain in China is complex and diverse, with undulating surfaces, and the overall characteristics are high in the west and low in the east. The main types of vegetation cover in China include grassland, evergreen coniferous forest, evergreen broad-leaved forest, deciduous broad-leaved forest, and farmland. China has a vast territory, a wide range of latitudes, and a large distance from the sea. In addition, the terrain has large ups and downs, and the terrain types and mountain ranges are diverse. Therefore, different combinations of temperature and precipitation have formed a variety of climates.

Combining the characteristics of solar-induced chlorophyll fluorescence and the spatial continuity of images, this study selects the Chinese mainland (excluding Hainan, Taiwan, Hong Kong, and Macao Special Administrative Regions) as the research area of this study to conduct downscaling research on SIF, as shown in Figure 1.
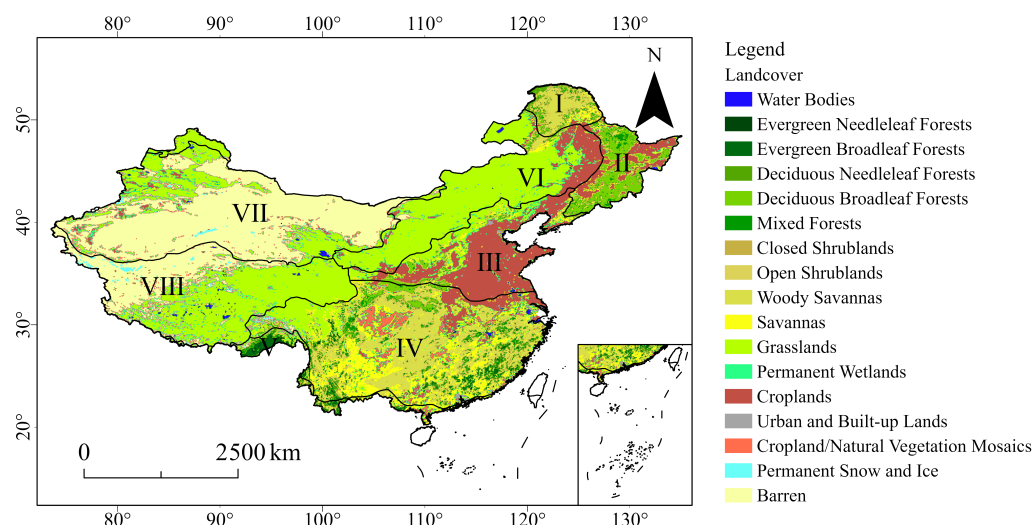
Figure 1. Study area. Numbers I–VIII in the figure represent: I. cold temperate deciduous coniferous forest area; II. temperate coniferous broadleaf mixed forest area; III. warm temperate deciduous broadleaf forest area; IV. subtropical evergreen broadleaf forest area V. tropical monsoon forest, rainforest area; VI. temperate grassland region; VII. temperate desert region VIII; alpine vegetation area of the Qinghai–Tibet Plateau.

2.2. Data

The data used in this study mainly include GOME-2 SIF products, surface reflectance products, and land cover products. These data will be used as input for the downscaling model.

The GOME-2 SIF product (https://avdc.gsfc.nasa.gov/pub/data/satellite/MetOp/GOME_F/v28/MetOp-A/level2/ (accessed on 10 June 2022)) is derived from 0.5° fluorescence data based on the MetOp-A satellite provided by the German Research Centre for Geosciences (GFZ).

The surface reflectance product (https://ladsweb.modaps.eosdis.nasa.gov/search/order/1/MCD43C4--6 (accessed on 10 June 2022)) is derived from MODIS Terra/Aqua data MCD43C4. It is a global 0.05° spatial resolution, 16-day temporal resolution surface reflectance dataset using the Bidirectional Reflectance Distribution Function (BRDF) with subsatellite reflectance adjustment, and contains the original MODIS data in reflectance bands 1 to 7.

The land cover product (https://ladsweb.modaps.eosdis.nasa.gov/search/order/1/MCD12C1--6 (accessed on 10 June 2022)) is the MODIS Land Cover Climate Modelling Grid (CMG) MCD12C1 version 6 data product, which is used in this study for the identification of vegetation cover areas in the terrestrial regions of China.

3. Method

3.1. Downscaling Algorithm

Currently, there are many methods for downscaling solar-induced chlorophyll fluorescence (SIF) data, such as using neural networks [8,16], tree-based methods [17], and semiempirical models [18] to generate high-resolution SIF products. The decision trees in the random forest algorithm randomly select a subset of features to split at each node, rather than using all features, so it can effectively predict the output variable even in the presence of multicollinearity (high correlation) among multiple input variables [19].

In this study, the surface reflectance data of seven bands of MCD43C4 in 2011 was used as the independent variable and the GOME-2 SIF as the dependent variable, and the random forest algorithm was used for training and testing. As the relationship between SIF and MODIS reflectance is considered to vary with biomes, climatic zones, and phenological stages, sample data with a spatial resolution of 0.5° were trained to better fit the environ-

mental cycle at a time step of each month in this study. At the same time, the sample data were randomly divided into 80% for training and 20% for testing, and the performance was found to be very close to each other, indicating that the prediction model in this study does not appear to have an overfitting phenomenon. In addition, we tested different models (number of trees and leaves), and we compared and analyzed the results of these model training results to select an optimal model. Then the obtained surface reflectance data of seven bands of MCD43C4 with a spatial resolution of 0.05° were used as the predicted independent variables to estimate the SIF data at 0.05° resolution for the land area of China in 2011.

3.2. Data Authenticity Test Method

Authenticity testing is the process of evaluating the accuracy of remote sensing products and analyzing their uncertainties through independent methods [20]. In this study, after generating downscaled SIF data at 0.05°, the data were verified for authenticity. There are two main methods that are usually used for verifying the authenticity of downscaled data: direct and indirect tests. However, it is currently difficult to verify the authenticity of the SIF dataset at the satellite scale by direct inspection methods. The reasons are mainly manifested in two aspects: first, SIF is a transient signal that varies with the incident light intensity, and there are great difficulties in synchronizing measurements with satellites, so there is a great difference in spatial scale between ground-based SIF data and satellite SIF remote sensing data, which cannot be directly compared [14]; secondly, due to the weakness of the SIF signal itself, it cannot be measured directly under natural light conditions and needs to be estimated by inversion with the help of various methods with uncertainties and incident irradiance [17], and the SIF signal is affected by atmospheric absorption and scattering on the satellite platform, which adds uncertainty factors to the SIF data set of the satellite platform [11]. Therefore, this study uses the cross-test method in the indirect test to test the accuracy of the downscaled SIF data by using the tested GOME-2 SIF data as the relative true value and employing the statistical methods of goodness of fit (R^2), Bias, root-mean-square error (RMSE), residual (δ), and relative error (RE). They are calculated as follows:

$$Bias = \frac{\sum_{i=1}^{n} M_i}{\sum_{i=1}^{n} N_i} - 1 \tag{1}$$

$$RMSE = \sqrt{\sum_{i=1}^{n} (M_i - N_i)^2 / n} \tag{2}$$

$$\delta = M_i - N_i \tag{3}$$

$$RE = \sum_{i=1}^{n} \frac{|M_i - N_i|}{N_i} \times 100\% \tag{4}$$

where M_i is the downscaled SIF at 0.05° resolution, N_i is the GOME-2 SIF at the original resolution of 0.5°, i is a specific pixel, and n is the total number of pixels.

4. Results and Analysis

4.1. Downscale Results

In this study, a downscaling method based on a random forest algorithm was proposed to downscale the 2011 GOME-2 SIF of the Chinese land area, resulting in SIF data at 0.05° spatial resolution. Figure 2 shows the distribution of GOME-2 SIF data for the Chinese mainland in 2011, and Figure 3 shows the distribution of downscaled SIF data in 2011. There are gaps in some areas of the study area due to the need for quality screening of data such as MCD43C4 during the data pre-processing stage.
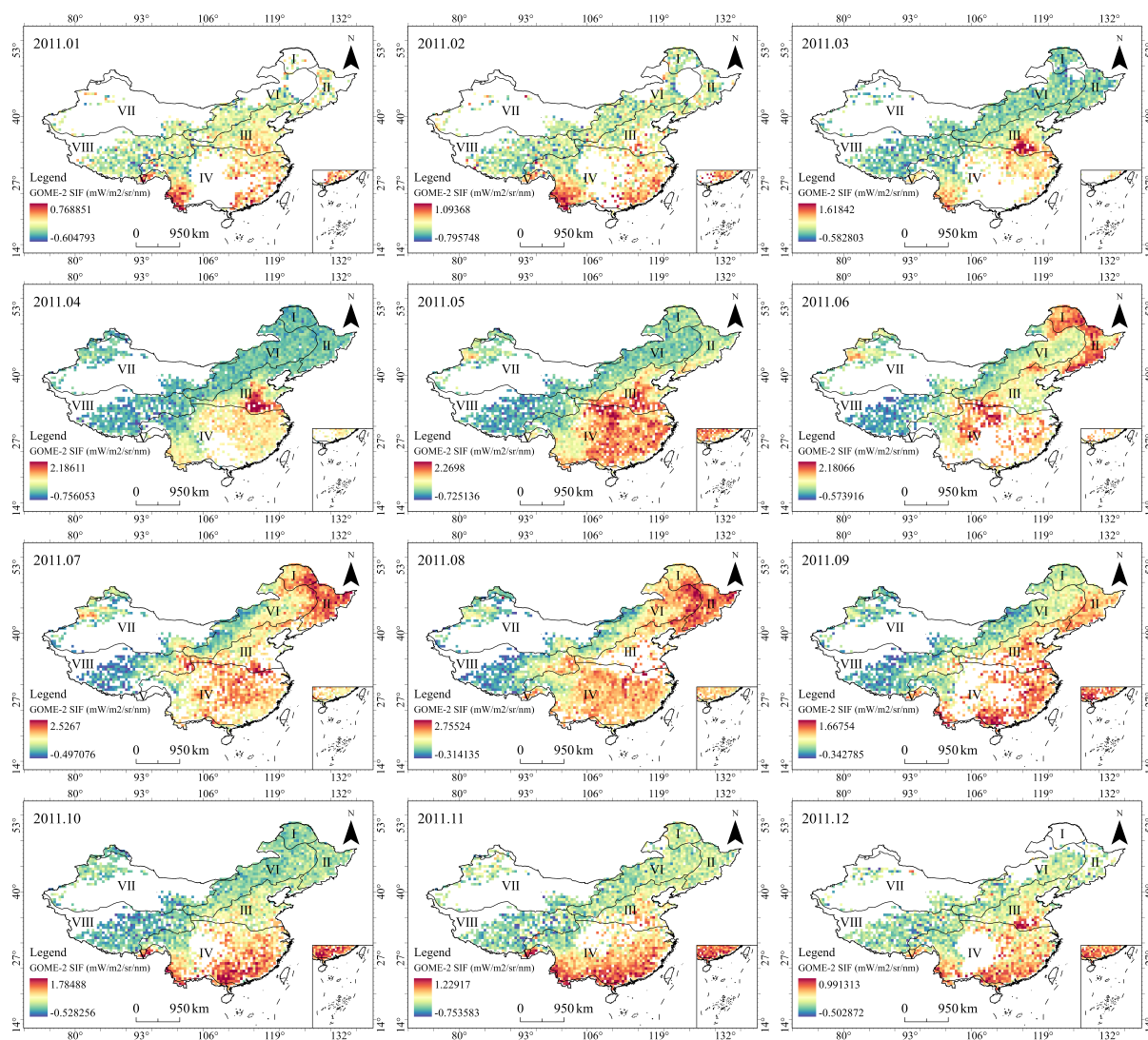
Figure 2. The 2011 GOME-2 SIF.

As can be seen from Figures 2 and 3, the spatial resolution of the downscaled SIF data has been significantly improved compared to the original GOME-2 product, and both the downscaled SIF data and the GOME-2 SIF data can reflect the obvious time-varying characteristics of the SIF. In terms of the spatial distribution of SIF, the descending scale SIF data and the spatial distribution of GOME-2 SIF are in good agreement, with both showing an overall decreasing trend from southeast to northwest. For example, fluorescence values in May 2011 were higher in most parts of China, mainly in the eastern and southern parts of China, which are the warm temperate deciduous broadleaf forest area and subtropical evergreen broadleaf forest area. The overall chlorophyll fluorescence intensity in November was low, with higher fluorescence values mainly in the southern part of China. These areas are mostly located in the subtropical evergreen broadleaf forest area, the tropical monsoon forest, and the rainforest area, where vegetation growth is more vigorous.
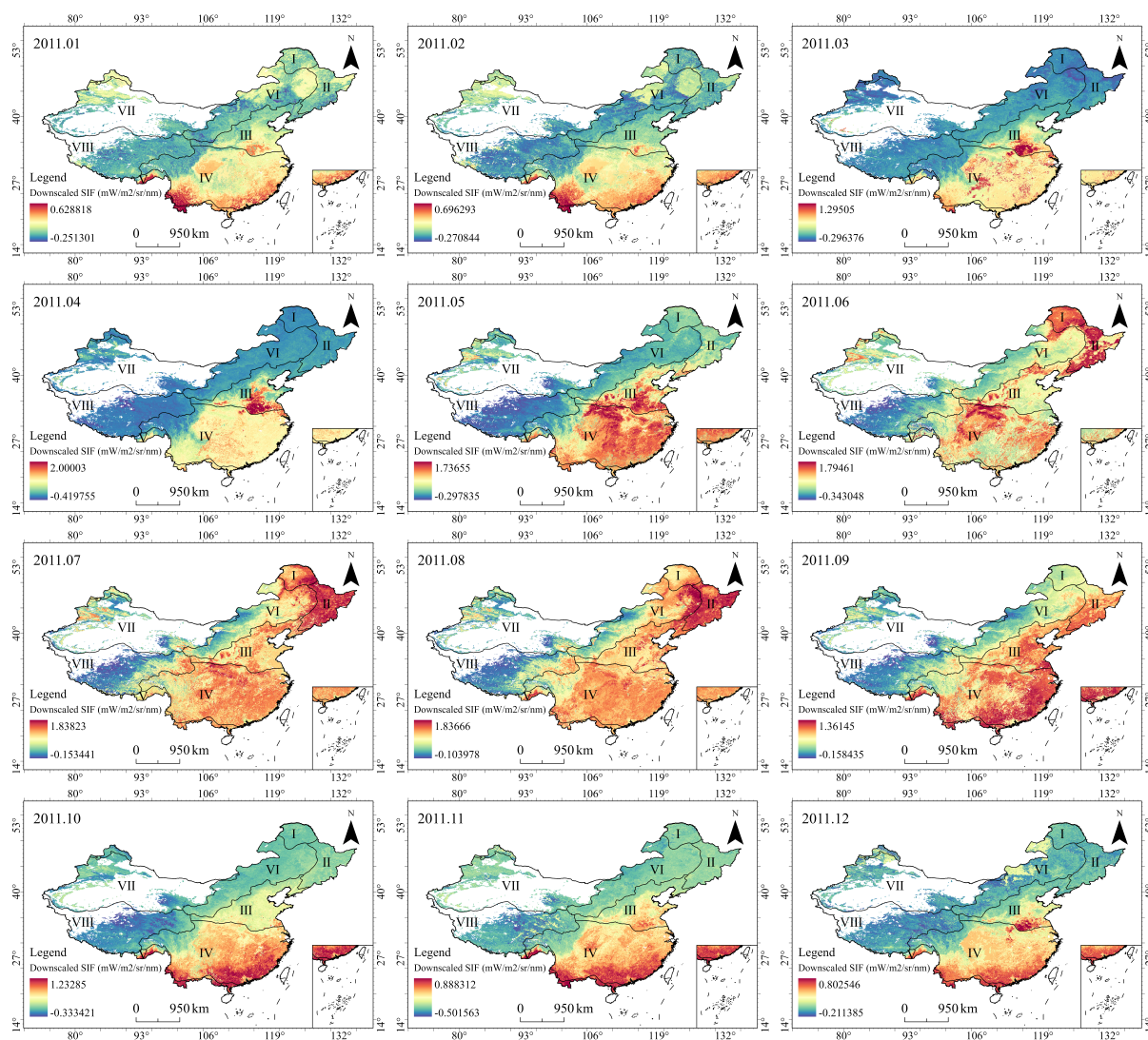
Figure 3. The 2011 downscaled SIF.

4.2. Data Authenticity Check

4.2.1. Monthly Scale Test

In order to better test the authenticity of the downscaled SIF data, the spatial resolution of the downscaled SIF data is resampled to 0.5°, and statistical methods such as goodness of fit (R^2), root mean square error (RMSE), and bias are used to assess the accuracy of the obtained downscaled SIF in combination with the GOME-2 SIF data. For comparison purposes, the downscaled SIF and GOME-2 SIF were normalized in this study and the results are shown in Table 1 and Figure 4. As can be seen from Table 1 and Figure 4, there is a good consistency between the 2011 downscaled SIF data and the GOME-2 SIF data on the monthly time scale. The downscaled SIF has a significant linear relationship with the GOME-2 SIF, and the downscaled SIF data retains the data characteristics of the GOME-2 SIF better. The R^2 on the monthly scale is above 0.4, especially in April–June and August, where it reaches above 0.8. The RMSE is distributed between 0.1034 and 0.1725 mW/m^2/sr/nm on the monthly scale. The Bias is less than 0 in January and May–October, indicating an underestimation in the downscaling of the GOME-2 SIF using MODIS data in these months.
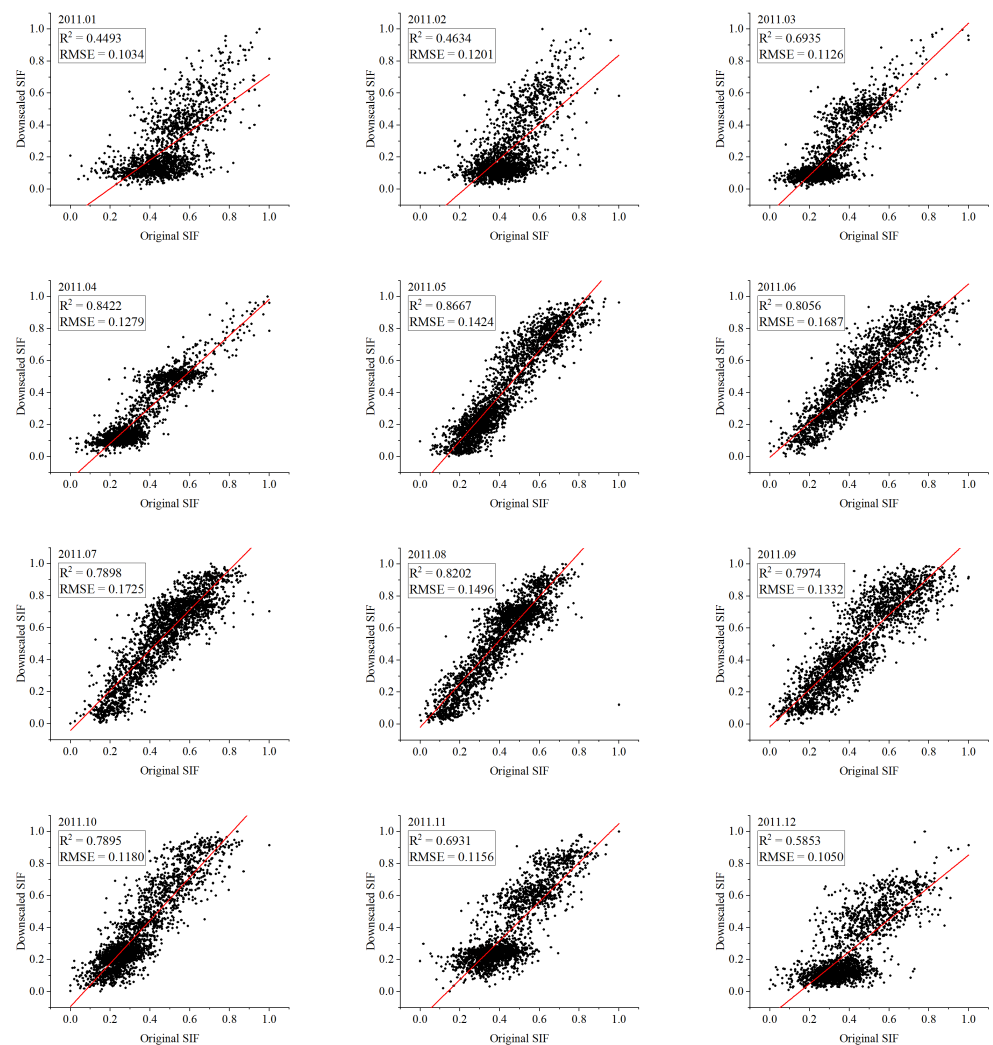
Figure 4. Monthly scale scatterplot of downscaled SIF data versus GOME-2 SIF data.

Table 1. Monthly scale authenticity test error evaluation index table.

Month	R^2	RMSE	Bias
1	0.4492 *	0.1034	−0.0425
2	0.4634 *	0.1201	0.0896
3	0.6935	0.1126	0.0446
4	0.8422	0.1279	0.0273
5	0.8667	0.1424	−0.0109
6	0.8056	0.1687	−0.0215
7	0.7898	0.1725	−0.0141
8	0.8202	0.1496	−0.0048
9	0.7974	0.1332	−0.0276
10	0.7895	0.1180	−0.0292
11	0.6931	0.1156	0.0471
12	0.5853	0.1050	0.0215

* in the table represents the poor statistical value of each indicator.

In order to evaluate the downscaled SIF results in more detail, this study calculated the residuals on the image element scale, as shown in Figure 5. We have classified the residuals in the categories shown in Table 2. The magnitude of the variation in the residuals determines the level of downscaling accuracy; the larger the range of variation of the residuals, the lower the accuracy. From Figure 5, it can be concluded that there was an obvious

underestimation phenomenon in the subtropical evergreen broad-leaved forest area from May to August 2011, which may be mainly due to the influence of local climate conditions. In summer, there is more cloudy and rainy weather in southern China. The generation of clouds may affect the accuracy of MODIS reflectance data, resulting in poor accuracy of downscaled SIF results.
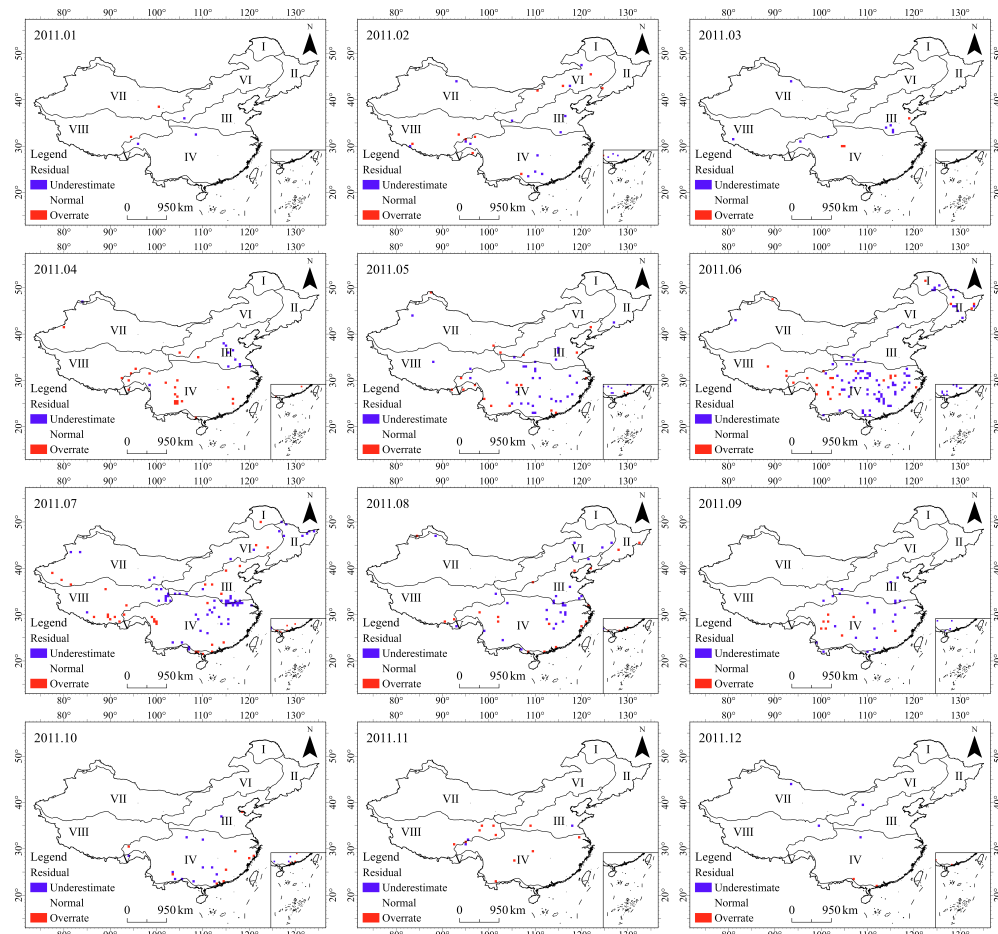

Figure 5. The 2011 prediction residuals.

Table 2. Monthly scale residual categories.

Residuals (mW/m^2/sr/nm)	Type
<-0.5	Underestimate
-0.5–0.5	Normal
>0.5	Overrate

4.2.2. Seasonal Scale Test

In order to study the accuracy of downscaled SIF data on a seasonal scale, this study divides March–May in 2011 into spring, June–August into summer, September–November into autumn, and January–February and December into winter. Table 3 is the authenticity test error evaluation index table for each season in 2011. Figure 6 is a scatter plot of downscaled SIF data and GOME-2 SIF data for each season in 2011. It can be seen from Table 3 and Figure 6 that on the seasonal scale, the correlation between the downscaled SIF and GOME-2 SIF is better than that on the monthly scale, with R^2 above 0.67, and the correlation in summer is the best, with R^2 being 0.8789. RMSE is distributed in the range of 0.0724–0.1212 mW/m^2/sr/nm on the seasonal scale. The Bias of spring, summer, and autumn are all less than 0, indicating that the downscaled SIF data are underestimated in these seasons.
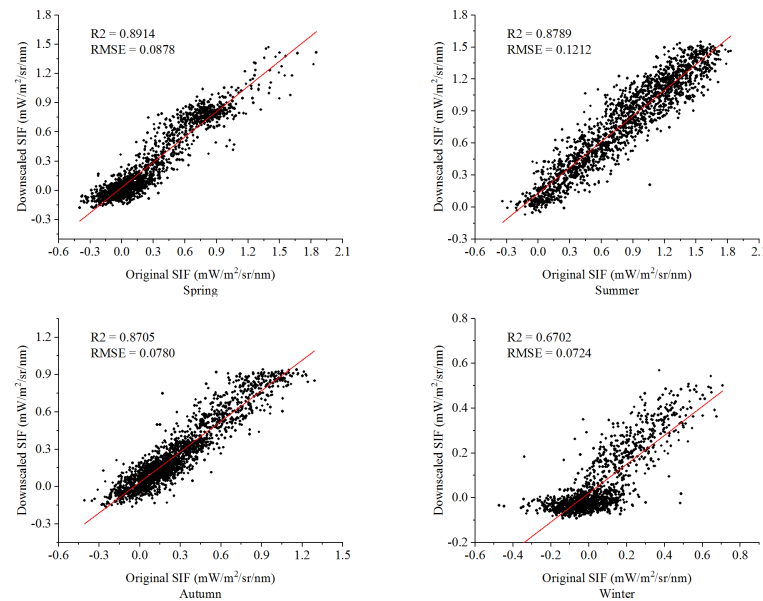
Figure 6. Seasonal scatterplot of downscaled SIF data versus GOME-2 SIF data.

Table 3. Seasonal scale authenticity test error evaluation index table.

Season	R^2	RMSE	Bias
Spring	0.8914	0.0878	−0.0161
Summer	0.8789	0.1212	−0.0379
Autumn	0.8705	0.0780	−0.0572
Winter	0.6702	0.0724	0.0194

4.3. Analysis of Factors Affecting the Accuracy of Downscaling Algorithms

The downscaling estimation of SIF has improved the spatial resolution of GOME-2 SIF from 0.5° to 0.05°, but the downscaling accuracy in some areas is still unsatisfactory, so it is necessary to analyze the factors that affect the downscaling accuracy. In this study, GOME-2 SIF and downscaled SIF data are used to calculate the relative error RE, and classify them, as shown in Table 4, and the spatial distribution is shown in Figure 7.

Table 4. RE classification.

RE	Type
<−80%	−1
others	0
>80%	1

4.3.1. SIF Data

Although the quality screening operation was performed on the original SIF data during data preprocessing, the distribution of SIF values in the real world itself has spatial heterogeneity, and SIF will have outliers, and the values will appear within the range of its effective values. However, the existence of points is significantly different from the average or common value. The existence of outliers will inevitably affect the downscaling results, resulting in higher or lower predicted values and surrounding SIF values [21]. Secondly, the real-world SIF itself has spatial heterogeneity, and the SIF distribution itself has outliers. If the real value is an outlier and the predicted value is a normal value, then there will be a large error in the prediction accuracy.
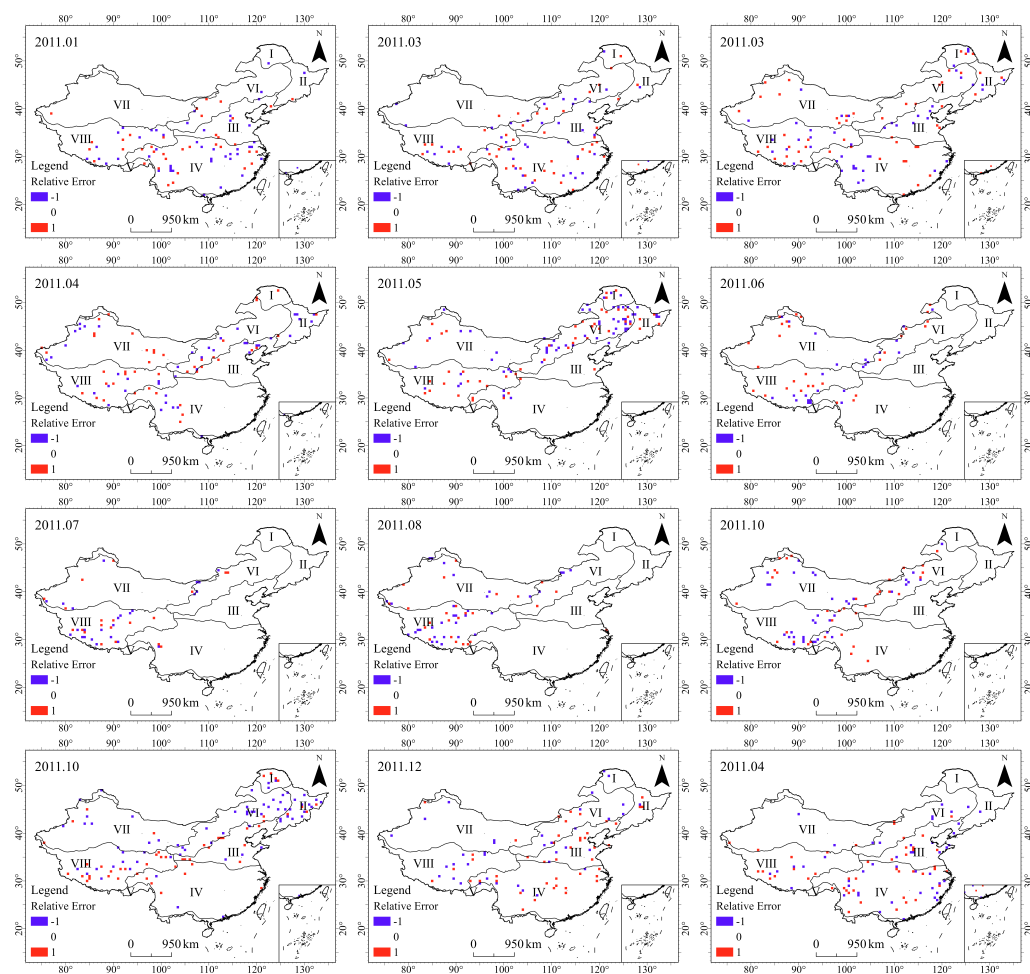
Figure 7. Monthly RE distribution chart.

4.3.2. Land Cover Types

Using MCD12C1 land cover data and monthly RE distribution data comprehensively, the land cover types corresponding to the points with large errors were extracted, as shown in Figure 8. It can be seen from Figures 7 and 8 that in 2011 the areas with large RE in each month have the distribution of grassland and barren types. Among them, grassland occupies a relatively large proportion, accounting for more than 40%. Especially in June, the error points where the land cover type is grassland accounted for about 80% of the total. Since special structural features of vegetation affect photosynthesis and plant growth, such as C3 and C4 plants and monocots and dicots, vegetation coverage levels may not fully represent light and action intensity levels. Yang [22] found that temperate and alpine grasslands in China exhibit different phenological and photosynthetic characteristics. Cui [23] found that the estimation of grassland phenology LSP indicators based on the MODIS vegetation index is most accurate within 18 days. The time resolution of the MODIS reflectance data used in this study is one month, so when the land cover type is grassland, it may affect the SIF downscaling accuracy.
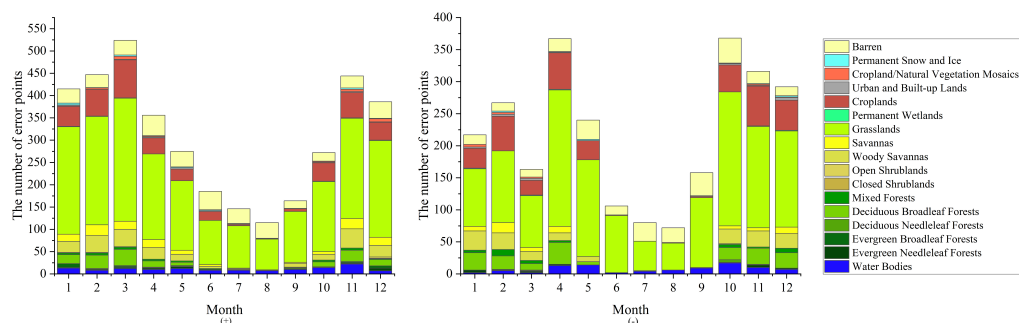
Figure 8. RE greater than 80% (**left**) and RE less than −80% (**right**) correspond to land cover types.

4.3.3. Climate Type

Using climate zone data and monthly RE distribution data comprehensively, the climate zone types corresponding to points with large errors are extracted, as shown in Figure 9. It can be seen from Figures 7 and 9 that the distribution of error points have obvious seasonal variation characteristics, with less distribution in summer and autumn and more distribution in winter and spring. The climatic regions where the error points are located also have obvious seasonal distribution characteristics. When the error point is negative, the spring is mainly concentrated in the warm temperate deciduous broadleaf forest area and the subtropical evergreen broadleaf forest area, accounting for 25% and 27%, respectively; the summer is mainly concentrated in the temperate grassland region, accounting for 37%; the autumn is mainly concentrated in the alpine vegetation area of the Qinghai–Tibet Plateau, accounting for 66%; winter is mainly distributed in the temperate desert region and alpine vegetation area of the Qinghai–Tibet Plateau, accounting for 16% and 25%, respectively. The error point is positive. In spring, it is mainly distributed in the subtropical evergreen broadleaf forest area, temperate grassland region, and alpine vegetation area of the Qinghai–Tibet Plateau, accounting for 24%, 25%, and 24%, respectively; in summer, it is mainly distributed in the temperate grassland region and the alpine vegetation area of the Qinghai–Tibet Plateau, accounting for 23% and 26%, respectively; autumn is mainly distributed in the temperate grassland region, temperate desert region, and alpine vegetation area of the Qinghai–Tibet Plateau, accounting for 26%, 26%, and 31%; in winter, they are mainly distributed in the temperate grassland region and the alpine vegetation area of the Qinghai–Tibet Plateau, accounting for 25% and 24%, respectively. In general, the temperate grassland region and the alpine vegetation area of the Qinghai–Tibet Plateau have the most error points, which will affect the accuracy of MODIS on the GOME-2 SIF downscaling results.
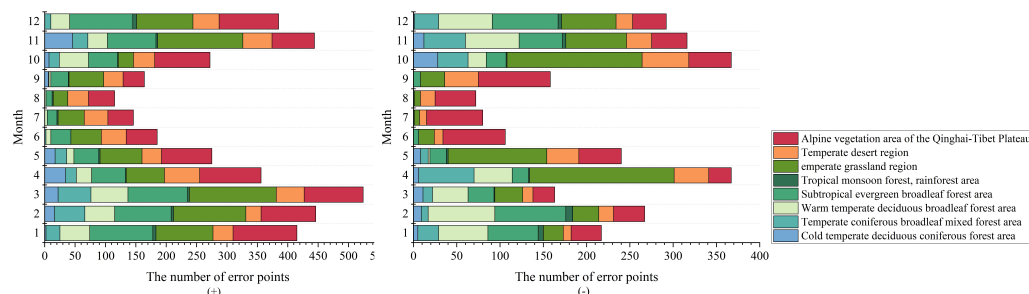

Figure 9. Climate zones corresponding to RE greater than 80% (**left**) and RE less than −80% (**right**).

4.3.4. DEM

Using DEM data and monthly RE distribution data comprehensively, the elevation values corresponding to points with large errors are extracted, as shown in Figure 10. It can be seen from Figures 7 and 10 that the highest DEM of the error point is at about 5600 m.

When the error point is negative, the average monthly DEM is mostly around 2000 m, but the average DEM from June to September is around 4000 m, and the median also shows the same pattern, and most of the error points are located at a higher DEM area; the error point is positive, the monthly DEM average is around 2400 m, and the median is around 2000 m. In areas with higher altitudes, the terrain is complex, and different slopes and slope directions receive different amounts of solar radiation. It is difficult to accurately represent the distribution of solar radiation on the ground [24], while the reflected radiation on the ground is part of the solar radiation. Therefore, in areas with high altitude and complex terrain, it is difficult for MODIS reflectance data to accurately represent the real situation, which will affect the results and generate errors during the SIF downscaling process.

Figure 10. DEM corresponding to RE greater than 80% (**left**) and RE less than −80% (**right**).

5. Conclusions

In this study, a method was proposed to downscale GOME-2 SIF data based on a random forest algorithm, and monthly SIF data with a spatial resolution of 0.05° in 2011 were generated. The authenticity of the downscaling results was tested. In addition, we analyzed the factors that may affect the accuracy of the downscaling results (land cover type, climate zone type, DEM). The following conclusions were drawn from the results that were obtained in this study:

(1) The accuracy of the downscaled SIF data obtained based on the downscaling algorithm is reliable, and has a strong consistency with GOME-2 SIF, and the spatial resolution of the data is higher. The results show that the spatial resolution and accuracy of the downscaled SIF data are better than those of the GOME-2 SIF data, the spatial resolution is increased from 0.5° to 0.05°, the overall R^2 is about 0.72, and the RMSE < 0.17.

(2) The accuracy of SIF downscaling results of grassland types is low.

(3) The temperate grassland region and alpine vegetation area of the Qinghai–Tibet Plateau can affect the accuracy of SIF downscaling results.

(4) Areas with high altitude and complex terrain will affect the downscaling results.

6. Discussion

We applied a random forest downscaling algorithm to process GOME-2 SIF data and generated downscaled SIF data products at a resolution of 0.05°. Meanwhile, we evaluated the accuracy of the downscaled SIF data at monthly and seasonal scales, and analyzed factors that may affect the downscaled accuracy. This study provides relevant assistance for the development of sun-induced chlorophyll fluorescence remote sensing, but there are still some shortcomings that need to be further explored in subsequent research.

Direct verification of downscaled SIF data faces challenges such as a lack of ground validation data and differences in temporal and spatial scales, which makes it difficult to

directly validate downscaled SIF data. In this study, we resampled the downscaled SIF data to the same spatial resolution as GOME-2 SIF data and indirectly cross-validated the data. The results showed that the two datasets have good consistency to some extent. Xing Li [14] conducted a downscaled study using OCO-2 SIF data and obtained 0.05° downscaled SIF data at the global scale, which also showed significant spatial correlation with the original SIF. Currently, most verification methods for downscaled data in research use ground station measurements for direct validation. However, due to the small proportion of chlorophyll fluorescence, which is a weak electromagnetic signal and only accounts for 1–2% of the surface reflection signal [25], it is difficult to capture and measure fluorescence near the ground. Therefore, there are limited ground data to validate SIF satellite data. The lack of ground measurement data will affect the accuracy of fluorescence products, which may limit the future development and application of fluorescence. Therefore, in order to validate SIF satellite data, it is necessary to expand the ground-based chlorophyll fluorescence observation system.

In addition, this study analyzed factors that may affect the accuracy of downscaling SIF, and the results showed that the regions with lower accuracy of downscaling SIF data are mainly concentrated in regions with land cover types of grassland, temperate steppe climate regions, alpine vegetation climate regions on the Qinghai–Tibet Plateau, and regions with complex terrain at higher altitudes. Since MODIS reflectance data vary among different land use types due to factors such as vegetation type, density, and land coverage [26], the regions with lower accuracy in this study are mainly concentrated in the northwestern region of China, where grasslands are the dominant vegetation cover type, which may be due to the impact of MODIS reflectance, resulting in lower accuracy. Therefore, it is necessary to focus on improving the SIF downscaling algorithm in these areas to improve data accuracy in the next research process or to distinguish these areas separately and find suitable SIF downscaling methods for these regions.

Overall, the downscaling algorithm proposed in this study has proven effective in improving the spatial resolution of GOME-2 SIF data while retaining its data characteristics. However, further research is needed to optimize the downscaling algorithm and explore its application in other regions.

References

1. Porcar-Castell, A.; Tyystjärvi, E.; Atherton, J.; Van der Tol, C.; Flexas, J.; Pfündel, E.E.; Moreno, J.; Frankenberg, C.; Berry, J.A. Linking chlorophyll a fluorescence to photosynthesis for remote sensing applications: Mechanisms and challenges. *J. Exp. Bot.* **2014**, *65*, 4065–4095. [CrossRef] [PubMed]
2. Mohammed, G.H.; Colombo, R.; Middleton, E.M.; Rascher, U.; van der Tol, C.; Nedbal, L.; Goulas, Y.; Pérez-Priego, O.; Damm, A.; Meroni, M.; et al. Remote sensing of solar-induced chlorophyll fluorescence (SIF) in vegetation: 50 Years of progress. *Remote Sens. Environ.* **2019**, *231*, 111177. [CrossRef] [PubMed]
3. Gupana, R.S.; Odermatt, D.; Cesana, I.; Giardino, C.; Nedbal, L.; Damm, A. Remote sensing of sun-induced chlorophyll-a fluorescence in inland and coastal waters: Current state and future prospects. *Remote Sens. Environ.* **2021**, *262*, 112482. [CrossRef]
4. Guanter, L.; Zhang, Y.; Jung, M.; Joiner, J.; Voigt, M.; Berry, J.A.; Frankenberg, C.; Huete, A.R.; Zarco-Tejada, P.; Lee, J.E.; et al. Global and time-resolved monitoring of crop photosynthesis with chlorophyll fluorescence. *Proc. Natl. Acad. Sci. USA* **2014**, *111*, E1327–E1333. [CrossRef] [PubMed]
5. Sun, Y.; Frankenberg, C.; Wood, J.D.; Schimel, D.; Jung, M.; Guanter, L.; Drewry, D.; Verma, M.; Porcar-Castell, A.; Griffis, T.J.; et al. OCO-2 advances photosynthesis observation from space via solar-induced chlorophyll fluorescence. *Science* **2017**, *358*, eaam5747. [CrossRef]
6. Joiner, J.; Yoshida, Y.; Vasilkov, A.; Yoshida, Y.; Corp, L.; Middleton, E. First observations of global and seasonal terrestrial chlorophyll fluorescence from space. *Biogeosciences* **2011**, *8*, 637–651. [CrossRef]
7. Liu, X.; Liu, L. GOSAT satellite remote sensing retrieval of chlorophyll fluorescence. *J. Remote Sens.* **2013**, *17*, 1518–1532.
8. Wen, J.; Köhler, P.; Duveiller, G.; Parazoo, N.; Magney, T.; Hooker, G.; Yu, L.; Chang, C.; Sun, Y. A framework for harmonizing multiple satellite instruments to generate a long-term global high spatial-resolution solar-induced chlorophyll fluorescence (SIF). *Remote Sens. Environ.* **2020**, *239*, 111644. [CrossRef]
9. Joiner, J.; Guanter, L.; Lindstrot, R.; Voigt, M.; Vasilkov, A.; Middleton, E.; Huemmrich, K.; Yoshida, Y.; Frankenberg, C. Global monitoring of terrestrial chlorophyll fluorescence from moderate spectral resolution near-infrared satellite measurements: Methodology, simulations, and application to GOME-2. *Atmos. Meas. Tech. Discuss.* **2013**, *6*, 3883–3930. [CrossRef]
10. Frankenberg, C.; O'Dell, C.; Berry, J.; Guanter, L.; Joiner, J.; Köhler, P.; Pollock, R.; Taylor, T.E. Prospects for chlorophyll fluorescence remote sensing from the Orbiting Carbon Observatory-2. *Remote Sens. Environ.* **2014**, *147*, 1–12. [CrossRef]
11. Köhler, P.; Frankenberg, C.; Magney, T.S.; Guanter, L.; Joiner, J.; Landgraf, J. Global retrievals of solar-induced chlorophyll fluorescence with TROPOMI: First results and intersensor comparison to OCO-2. *Geophys. Res. Lett.* **2018**, *45*, 10–456. [CrossRef]
12. Yu, L.; Wen, J.; Chang, C.; Frankenberg, C.; Sun, Y. High-resolution global contiguous SIF of OCO-2. *Geophys. Res. Lett.* **2019**, *46*, 1449–1458. [CrossRef]
13. Duveiller, G.; Filipponi, F.; Walther, S.; Köhler, P.; Frankenberg, C.; Guanter, L.; Cescatti, A. A spatially downscaled sun-induced fluorescence global product for enhanced monitoring of vegetation productivity. *Earth Syst. Sci. Data* **2020**, *12*, 1101–1116. [CrossRef]
14. Li, X.; Xiao, J. A global, 0.05-degree product of solar-induced chlorophyll fluorescence derived from OCO-2, MODIS, and reanalysis data. *Remote Sens.* **2019**, *11*, 517. [CrossRef]
15. Hu, S.; Mo, X. Detecting regional GPP variations with statistically downscaled solar-induced chlorophyll fluorescence (SIF) based on GOME-2 and MODIS data. *Int. J. Remote Sens.* **2020**, *41*, 9206–9228. [CrossRef]
16. Gentine, P.; Alemohammad, S. Reconstructed solar-induced fluorescence: A machine learning vegetation product based on MODIS surface reflectance to reproduce GOME-2 solar-induced fluorescence. *Geophys. Res. Lett.* **2018**, *45*, 3136–3146. [CrossRef]
17. Ma, Y.; Liu, L.; Chen, R.; Du, S.; Liu, X. Generation of a global spatially continuous TanSat solar-induced chlorophyll fluorescence product by considering the impact of the solar radiation intensity. *Remote Sens.* **2020**, *12*, 2167. [CrossRef]
18. Duveiller, G.; Cescatti, A. Spatially downscaling sun-induced chlorophyll fluorescence leads to an improved temporal correlation with gross primary productivity. *Remote Sens. Environ.* **2016**, *182*, 72–89. [CrossRef]
19. Gómez-Ramírez, J.; Ávila-Villanueva, M.; Fernández-Blázquez, M.Á. Selecting the most important self-assessed features for predicting conversion to mild cognitive impairment with random forest and permutation-based methods. *Sci. Rep.* **2020**, *10*, 20630. [CrossRef]
20. Justice, C.; Belward, A.; Morisette, J.; Lewis, P.; Privette, J.; Baret, F. Developments in the 'validation' of satellite sensor products for the study of the land surface. *Int. J. Remote Sens.* **2000**, *21*, 3383–3390. [CrossRef]
21. Shen, S.; Zhao, J.; Jia, J.; Zhao, Y. Comparison of different methods for downscaling TRMM precipitation data in Qilian Mountains. *J. Mt. Sci.* **2019**, *37*, 923–931.
22. Yang, J.; Xiao, X.; Doughty, R.; Zhao, M.; Zhang, Y.; Köhler, P.; Wu, X.; Frankenberg, C.; Dong, J. TROPOMI SIF reveals large uncertainty in estimating the end of plant growing season from vegetation indices data in the Tibetan Plateau. *Remote Sens. Environ.* **2022**, *280*, 113209. [CrossRef]
23. Cui, T.; Martz, L.; Zhao, L.; Guo, X. Investigating the impact of the temporal resolution of MODIS data on measured phenology in the prairie grasslands. *GISci. Remote Sens.* **2020**, *57*, 395–410. [CrossRef]
24. Li, J.; Luo, J. Simulation of solar radiation in mountainous areas under clear sky. *Geogr. Arid. Reg.* **2015**, *38*, 120–127.

25. Meroni, M.; Rossini, M.; Guanter, L.; Alonso, L.; Rascher, U.; Colombo, R.; Moreno, J. Remote sensing of solar-induced chlorophyll fluorescence: Review of methods and applications. *Remote Sens. Environ.* **2009**, *113*, 2037–2051. [CrossRef]
26. Zhang, X.; Friedl, M.A.; Schaaf, C.B.; Strahler, A.H.; Hodges, J.C.; Gao, F.; Reed, B.C.; Huete, A. Monitoring vegetation phenology using MODIS. *Remote Sens. Environ.* **2003**, *84*, 471–475. [CrossRef]